International Journal of Engineering & Technology, 7 (4.27) (2018) 73-77

International Journal of Engineering & Technology

Website: www.sciencepubco.com/index.php/IJET

Research paper

Title of the Integrity Analysis of O&G Standpipe Separator: Numerical Study Article

Mohd Faizal Hakim Hidzir[1], Khairul Imran Sainan[2]*, Hazran Husain[3]

[1,2,3] *Fakulti Kejuruteraan Mekanikal UiTM*
**Corresponding author E-mail: imransainan@salam.uitm.edu.my*

Abstract

A standpipe is a component that functions to remove the condensate of gas from the oil that flows inside the O&G piping system underneath. Efficient gas removal promotes better crude oil quality and increases productivity. The deflector plates integrity in a stand pipe, where thin plates are mounted on the pipe walls periodically in the direction of fluid flow, has been numerically investigated. The aim of this investigation is to determine how the working fluid density and deflectors thickness influenced the plates integrity. Two working fluids were tested. Natural gas and crude oil which has a higher density. The thickness of the plates was 3 mm and 6 mm. A series of simulation analyses were done analytically through CFD and FEA simulation method using ANSYS software. Based on the results, crude oil produces higher stress onto the plates. This causes large plate deflection. It was observed, the plates near to the standpipe inlet were subjected to the highest stress. Stress on the deflector plates drops as the fluid travel along the pipe height. The deflector plates of 3 mm were failed under these conditions and were not recommended for usage.

Keywords: *Pressure distribution; Deformation; Plate Thickness; Density of oil/gas; CFD and FEA*

1. Introduction

O&G standpipe is a component use in natural gas condensate removal processes in a gas processing plant. The standpipe upstream is attached to the O&G piping system and downstream to the atmosphere. The natural gas is treated as it flows along the standpipe separating the oil from water vapor and condensable hydrocarbons or called condensate. A standpipe is actually a baffled channel flow. The separation process depends on the baffle plates mounted on the pipe walls periodically in the direction of fluid flow. The condensate is separated from the oil due to having lower density and flows out of the pipes. The oil at higher density, restricted by the plates flows back into the O&G piping underneath. The plates are subjected to a high convective force due to the fluid flows instability in the pipes. Therefore, understanding the limitation of the plates is very important in fluid separation process, and must be preceded by a study of the flow instability associated with turbulent and mixing flow configuration.

Flows in standpipe or separators are often characterized by the plates. Similar fluid flows concept is used in a shell and tube heat exchanger (STHX) system. Baffles or plates are located inside the shell along the main flow. The application of baffles in the STHX system is to increase fluid mixing for heat transfer activity. Past studies have reported, the heat transfer performance of the STHX with baffles is greater to the non-baffled STHX. The analysis was done numerically using commercially available CFX4.2 [1]. Similar numerical analysis was conducted to investigate the complex flow and temperature pattern in a short shell and tube type heat exchanger, with and without baffles in the shell side[2]. The spacing, angle and plates cut determines the structure of the stream. The influence of plate spacing for example and Reynolds number (Re) towards flow instability has been well explained [3]. The helical baffles or plates employ in STHX system with different angles of 8^0, 12^0, 20^0, 30^0 and 40^0 configurations shows different flows occurrence and contributes towards the baffles performance [4]. Baffle cut is also identified as an important geometric parameter effecting heat transfer and pressure drop. The effect of baffle spacing was analyzed as well[5][6]. The pressure drop decreased as the baffle spacing decreased, but for a fixed stream-wise length, the pressure drop was slightly larger for smaller spaces [7].

This shows that, the plates configurations mounted on the wall disturb the fluid motions and destabilizing the flow field. Consequently, turbulent and mixing flows are greatly increases, resulting in variation of pressure drop[8]. This type of flows condition is constantly subjected towards the thin deflector plates thus may causes plates failure.

In this project, the integrity of the stand pipe plates has been identified by computational fluid dynamics (CFD) and Finite Element Analysis (FEA) method. The commercial software ANSYS was used and all computations were performed on a personal computer with 16GB RAM and Intel Core i7-2600 at 3.60 GHz CPU. The results were presented in a graphical manner for comparison purposes.

2. Nomenclature of a Stand Pipe

The standpipe mainly consists of two components which are a flange pipe and deflector plate lining pipe as shown in Figure 1. The pipe flange is located at the outer side of the standpipe. The material properties of the flange pipe were kept constant. The critical component is the deflector plates lining which is located inside the standpipe. This component is exposed to the fluid flow during the condensate process. The deflector plate function is to filter out the condensate gas. The deflector plates will capture oil droplets and flow the oil back into the pipeline. The thickness of

the plate and the fluid density flow is varied to identify the integrity of the standpipe.

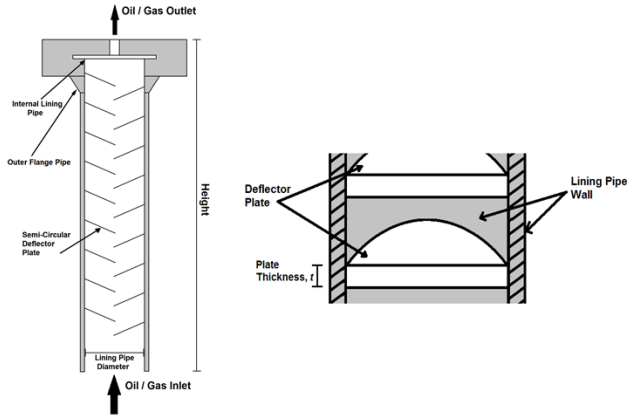

Fig. 1: Nomenclature of a stand pipe and deflector plate

3. Factors Influenced the Stand Pipe Integrity

Factors identified that influenced the integrity of a standpipe. The pipe material, size such as diameter and height, the deflector thickness and working fluid. Higher strength material is preferred for the standpipe robustness. The standpipe height increases the pipe head. The distance between deflectors on the other hand plays a significant role towards the pressure distribution within the pipe. The deflectors spacing and cut determines the structure of the stream. In this project, two variables were considered; the deflectors thickness and the working fluids.

3.1. Deflector Plate Dimensions

The height of the standpipe is 2.5 m with a diameter of 370 mm. The minimum angle of deflection is 600 and the distance between the plates are 170 mm. The plates are semi-circular in configurations. The deflector thickness is 3 mm and 6 mm.

3.2. Fluid Density and Viscosity

The working fluid analyzed is natural gas and crude oil. Therefore, fluid density and viscosity setting were varied. Natural gas has relatively low density compared to crude oil. In reality, both fluids are simultaneously operated inside the pipes. Thus, the effect of two-phase flow should be considered. However, in this project, an assumption was made. The natural gas and crude oil were tested separately during the analysis. The results of pressure variation for each fluid during the CFD analyses were taken directly and applied onto the FEA analyses.

3.3. Material of Pipes

The material of the flange pipe is carbon steel, ASTM A105N. The yield's strength and tensile strength of the carbon steel is 248 MPa and 483 MPa respectively. For the lining pipe inside the flange pipe, the material is stainless steel, SS316. The yield's strength and tensile strength of the stainless steel is 205 MPa and 515 MPa respectively. The material properties of the standpipe are important as it becomes the base judgment for deflector plate failure. Higher material properties would enhance the strength of the standpipe. However, this parameter was kept constant throughout the analyses.

4. Modeling

In this study, the flange pipe is ignored. The fluid domain mainly focuses towards the inner pipe of deflector lining pipe. The geometric models with 18 deflector plates is shown in Fig. 1. The properties of natural gas and crude oil are defined as constants and were manually inserted into the Fluent.

4.1. Governing Equations

The governing equations are modified according to 3D incompressible base flow. The simulated cases is assumed to be steady. The time dependent terms are dropped from the equations. The system occurs without heat transfer and assume adiabatic process. The resulting equations are:

Conservation of mass:

$$\frac{\partial \rho}{\partial t} + \frac{\partial \rho u_j}{\partial x_j} = 0 \tag{1}$$

Conservation of momentum:

$$\frac{\partial}{\partial t}(\rho u_i) + \frac{\partial}{\partial x_j}\left[\rho u_i u_j + p\delta_{ij} - \tau_{ji}\right] = 0 \tag{2}$$

The fluid flow is turbulent. The Reynolds number more than 10,000. Therefore, turbulence modeling was used to account for the effects of turbulence. In the analysis of CFD for STHX with and without baffles, standard k-ε model was used. The model is a two-equation model of semi-empirical based transport equations. The turbulence kinetic energy, k and the turbulence dissipation rate, ε. The results produced almost 20 percent accuracy [2]. In a small STHX of 6 equally spaced baffles simulation. Three models were used. The Spallart Almaras, the standard k- ε and the realizable k-e model. The Spallart Almaras only solved for one turbulence equation. The realizable k-ε includes a new formulation for turbulent viscosity in the realizable model and different derivation for transport equation in the dissipation rate. The k-ε realizable model gave the best agreement compared to Spallart-Almaras model and standard k-ε model[6]. Analysis of continues helical FRP baffles in STHX considers three different turbulence model. The models included were realizable k-ε, standard k-ε and SST k-ω. The k-ε realizable model showed good agreement with experimental results with 8 percent accuracy [9]. Therefore, in this study, realizable k-ε model was used. The formulation of the model equation for steady state 3D incompressible flow are as follows:

$$\frac{\partial}{\partial t}(\rho k) + \frac{\partial}{\partial x_j}(\rho k u_j) = \frac{\partial}{\partial x_j}\left[\left(\mu + \frac{\mu_t}{\sigma x_k}\right)\frac{\partial k}{\partial x_j}\right] + G_k + G_b - \rho\varepsilon - Y_M + S_k \tag{3}$$

$$\frac{\partial}{\partial t}(\rho\varepsilon) + \frac{\partial}{\partial x_j}(\rho\varepsilon u_j) = \frac{\partial}{\partial x_j}\left[\left(\mu + \frac{\mu_t}{\sigma_\varepsilon}\right)\frac{\partial \varepsilon}{\partial x_j}\right] + \rho C_1 S\varepsilon + \rho C_2 \frac{\varepsilon^2}{k + \sqrt{v\varepsilon}} + C_{1\varepsilon}\frac{\varepsilon}{k}C_{3\varepsilon}G_b + S_\varepsilon \tag{4}$$

4.2. Linear Momentum Equation

Linear momentum equation [10],

$$\frac{\partial}{\partial t}\int_{cv} v\rho dV + \int_{cs} v\rho V \cdot \hat{n} dA = \sum F \tag{5}$$

The first term of the Equation 1, was cancelled out since the flow was assumed as steady. Hence the equation can be simplify into:

$$\int_{cs} v\rho V \cdot \hat{n} dA = \sum F \tag{6}$$

From Equation 2, consider the force acting on deflector plate is due to the momentum force of the fluid. To determine the pressure acting on the plate, the equation can be generalize into:

$$P_{act} = \frac{F}{A} \tag{7}$$

Equation 3 is the general equation used to determine the pressure acting on the deflector plate by using the reaction from the momentum force of the fluid, F divide with the area at each point of the deflector plates [9].

$$\Delta p = f \frac{L}{D} 2\rho v^2 \tag{8}$$

Equation 4 is the equation for pressure losses across the pipe. Based on the equation, the parameters that affect the pressure losses in the pipe is friction factor, f, and the length of the pipe, L, the diameter of the pipe, D, density, ρ and velocity of fluid, V. In the CFD analysis, the only parameter change was the density of fluid while other parameters were kept constant.

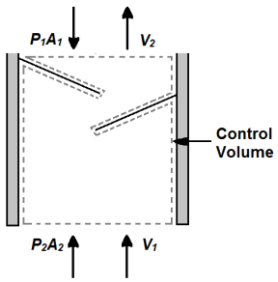

Fig. 3: Pressure drop across the stand pipe

4.3. Stress on Deflector Plates

Stress at edge,

$$\sigma_m = \frac{3pr^2}{4t^2} \tag{9}$$

Deflection at center,

$$y_m = \frac{0.171pr^4}{Et^3} \tag{10}$$

The equation (9) and (10) shows the maximum stress and deflection of the semi-circular plates. It is subjected to the distributed loads which are the fluid pressure with the fixed edge around the semicircle. The maximum stress, σm is the relation between the product of pressure, p with the power of radius, r over the deflector plate thickness, t. The maximum deflection, ym usually located at the center of the plate which relates the product of flexural rigidity coefficient with pressure and radius over the product of young's modulus, E on the plate thickness [10, 11].

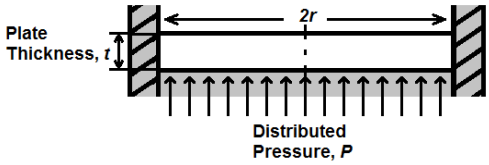

Fig. 4: Circular plate stress and deformation parameters

4.4. Boundary Conditions

The simulations were separated into four different cases varied in terms of deflector thickness and working fluids. The inlet velocity was kept constant. The model requires 1.2 million grid meshes of tetrahedral elements. Near wall treatment was applied towards the wall especially on the thin wall plates. The no-slip condition was employed at all solid boundaries. Assuming the wall is perfectly insulated, zero heat flux is assigned. The inlet temperature assumption is 320 K. The standpipe downstream is assigned as zero gauge pressure to formulate the atmospheric pressure value. Uniform velocity is assumed towards the standpipe entrance. For pressure-velocity coupling, SIMPLE method was used. Second order upwind scheme was used to discretize the convective terms in all boundaries. The convergence criterion was kept at 10^{-4} for the flow residuals. The physical condition setting applied is shown in Table 1.

Table 1: CFD Inputs and Boundary Conditions

Parameters	Case A	Case B	Case C	Case D	Unit
Velocity inlet	7.9	7.9	7.9	7.9	m/s
Working fluid	Natural gas	Crude oil	Natural gas	Crude oil	-
Deflector thickness	3	3	6	6	mm
Fluid density	0.712	51.695	0.712	51.695	kg/m^3
Deflector angle	60	60	60	60	^{0}
Deflectors	170	170	170	170	mm
Pipe Height	2500	2500	2500	2500	mm
Pressure outlet	101325	101325	101325	101325	Pa

5. Results and Discussions

5.1. Pressure Drop along the Pipes

The results obtained from the CFD analysis is shown in Figure 5. In this figure, the results represent the distribution of pressure along the standpipe. Overall, pressure was varied depending on the fluid properties. The graph of pressure versus the number of deflector plates is plotted as shown in Figure 6. The highest pressures occurred across cases A, B, C and D were 0.848, 10.81, 0.845 and 12.05 MPa respectively. Meanwhile, the lowest pressures recorded were 0.832, 9.430, 0.829 and 10.24 MPa. Pressure on the deflectors drops as the fluid travel along the pipe height. The highest pressure was found on the deflector near the pipe inlet. The lowest pressure occurred on the farthest plates located at the pipes downstream. The minimum pressures resulting in almost 8 times larger than the atmospheric pressure. The deflector plates, obstructs the fluid motion causes flow separation near the plates edge. This results in large pressure drop inside the pipes thus requires higher pumping power [11]. Under this condition, the plates were subjected with large convective force as the fluid travels out of the standpipe. Based on linear momentum equation [10], assuming fixed control volume, as the pressure drop increases the convective force acted onto the plates is increases. Refer equation (5) and Figure 3. The continuous loading onto the plates induced plates vibration thus shorten the operational lifetime [12] [13].

5.2. Effect of Working Fluids

Based on Figure 6, it is clearly shown that pressures on deflector plates were depending on the working fluids. Crude oil produces higher pressure compare to natural gas. This is because of density. Higher density increases the mass flow rate thus increasing the momentum of fluid within the pipes. The momentum of fluid changes is in direct proportion to the density. As stated in equation (6), since cross-sectional area and velocity were kept con-

stant. The density became the dominant factor in momentum changes. It worth stated here, the thickness of deflector plates did not have any role in momentum changes at all. It shows that pressure difference between pipes A and C did not deviate even though the plate thickness is different. A similar pattern was observed for pipes B and D. The difference in pressure between the pipes were 12.6 and 1.89 percent respectively.

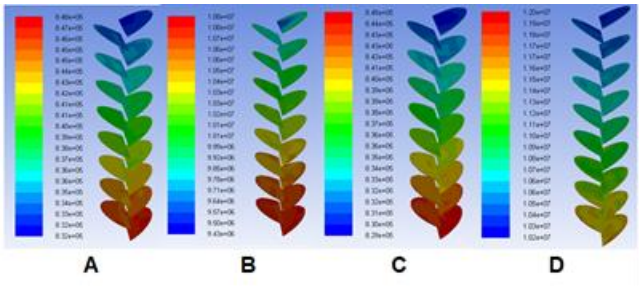

Fig. 5: Absolute pressure contour on deflector plate

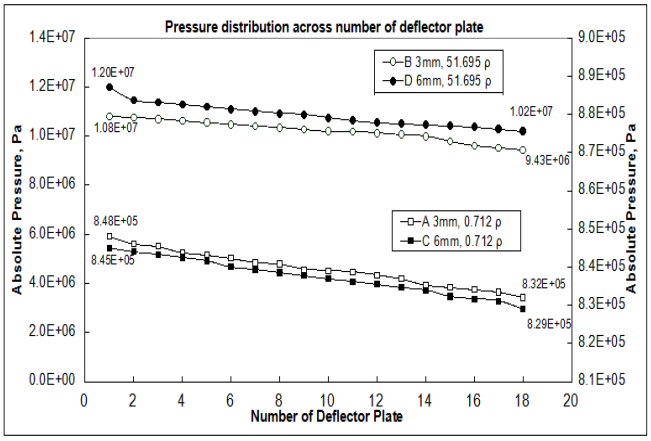

Fig. 6: Pressure distribution across number of deflection plate

5.3. Stress and Deformation

The results obtained from the FEA analysis is shown in Figure 7. In this figure, the result of stress, strain and deformation of the deflector plate is presented. The deformation can be seen clearly occurred at the center of deflection plate and decreases near to the pipes lining. The stress and strain was observed to be occur at the fixed edge of the plate. The maximum value of deformation and stress for each plate was taken by using probe tool to plot the chart as shown in figure 8 and figure 9. The x-axis represent the number of deflector plate and y-axis represent the deformation and stress.

Based on the results, there are huge different of deformation and stress between the difference of plate thickness and fluid properties. From result B, it show the highest value due to the high force from the fluid properties and the small dimension of the plate. The maximum deformation and stress is 20.07 mm and 1387.1 MPa respectively. Followed by result D, the maximum deformation and stress is 5.14 mm and 481.31 MPa respectively. For result C, the maximum deformation of plate is 0.63 mm while the maximum of stress is 36.78 MPa. From result A, the maximum deformation and stress is 0.0164 mm and 2.14 MPa respectively. As we can see the result shown the smallest value of deformation and stress. This is due to the greater thickness of deflector plate and the lower pressure force from the fluid properties.

To identify the best case for the stand pipe operation, the resultant stress for each cases was compared to the ultimate tensile stress of the lining pipe which is 515 MPa. By comparing the maximum stress, result B was highly exceed the ultimate tensile stress which is 1387.1 MPa where it is 37.1% greater. Under this condition, the plate is expected to fail. For result D, the maximun stress is 481.31 MPa and 6.5% lower than the ultimate tensile strength of the lining pipe. Although it is lower compared to B, and meet the strength requirement, the plate under this condition consider as fail because of safety factor. As for result C and A, the maximum stress is lower than the ultimate tensile strength by 92.8% and 99.5% respectively. Both plates under these conditions consider as safe.

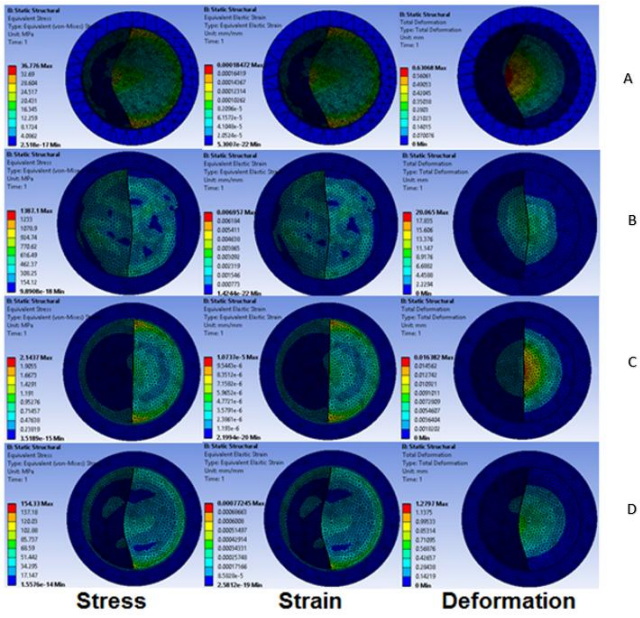

Fig. 7: Stress, Strain and Deformation

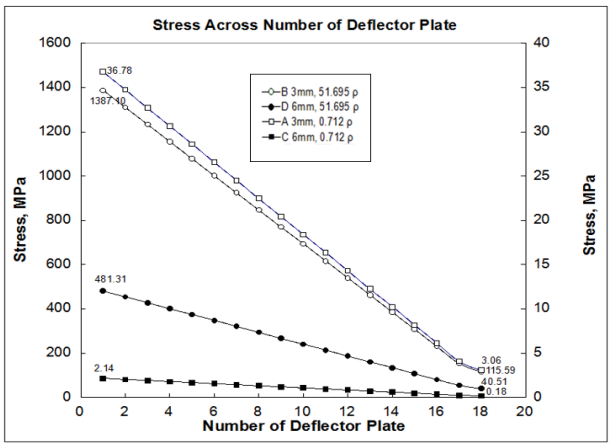

Fig. 8: Stress across Number of Plates

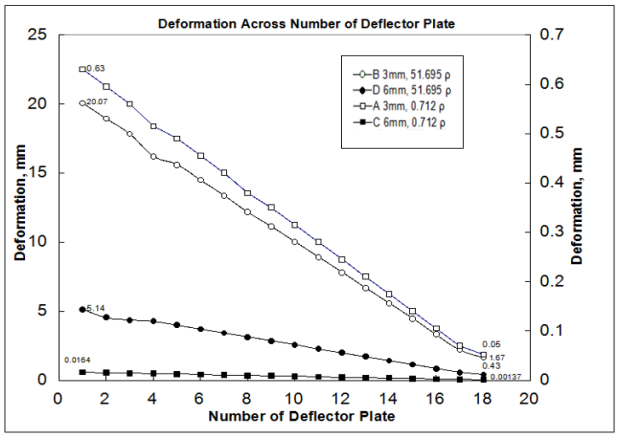

Fig. 9: Deformation across Number of Plate

6. Conclusion

Based on the CFD and FEA analysis of the pressure distribution and the deformation of the deflector plate, we can make a few

conclusions. From CFD analysis, the fluid density affected the pressure distribution throughout the internal part of the stand pipe. The pressure distribution was taken from the surface area of the deflector plate pipe lining. For FEM part, we can conclude that the greater the thickness of deflector plate reduces the stress and strain and also the total deformation of the deflector plate. To conclude the overall project, we can say that the stand pipe could only run with low density fluid such as the natural gas. It is clearly to say that the high density fluid such as the crude oil will cause deflector plate failure. Therefore, the plate thickness must be increased.

References

[1] Y.-S. Son and J.-Y. Shin, "Performance of a shell-and-tube heat exchanger with spiral baffle plates," *KSME Int. J.*, Vol. 15, No. 11, (2001), pp. 1555–1562.

[2] E. Pal, I. Kumar, J. B. Joshi, and N. K. Maheshwari, " CFD simulations of shell-side flow in a shell-and-tube type heat exchanger with and without baffles," *Chem. Eng. Sci.*, Vol. 143, (2016), pp. 314–340.

[3] C. Kang and K.-S. Yang, "Flow instability in baffled channel flow," *Int. J. Heat Fluid Flow*, Vol. 38, (2012), pp. 40–49.

[4] B. Gao, Q. Bi, Z. Nie, and J. Wu, "Experimental study of effects of baffle helix angle on shell-side performance of shell-and-tube heat exchangers with discontinuous helical baffles," *Exp. Therm. Fluid Sci.*, Vol. 68, (2015), pp. 48–57.

[5] D. Eryener, "Thermoeconomic optimization of baffle spacing for shell and tube heat exchangers," *Energy Convers. Manag.*, Vol. 47, No. 11–12, (2006), pp. 1478–1489.

[6] E. Ozden and I. Tari, "Shell side CFD analysis of a small shell-and-tube heat exchanger," *Energy Convers. Manag.*, Vol. 51, (2010), pp. 1004–1014.

[7] E. M. Sparrow and L. G. Reifschneider, "Effect of interbaffle spacing on heat transfer and pressure drop in a shell-and-tube heat exchanger," *Int. J. Heat Mass Transf.*, Vol. 29, No. 11, (1986), pp. 1617–1628.

[8] S. Zeyninejad Movassag, F. Nemati Taher, K. Razmi, and R. Tasouji Azar, "Tube bundle replacement for segmental and helical shell and tube heat exchangers: Performance comparison and fouling investigation on the shell side," *Appl. Therm. Eng.*, Vol. 51, No. 1–2, (2013), pp. 1162–1169.

[9] S. Shinde and U. Chavan, "Numerical and experimental analysis on shell side thermo-hydraulic performance of shell and tube heat exchanger with continuous helical FRP baffles," 2018.

[10] P. M. Gerhart, A. L. Gerhart, and J. I. Hochstein, *Munson's fluid mechanics*. John Wiley & Sons, (2017).

[11] A. S. Ambekar, R. Sivakumar, N. Anantharaman, and M. Vivekenandan, "CFD simulation study of shell and tube heat exchangers with different baffle segment configurations," *Appl. Therm. Eng.*, Vol. 108, (2016), pp. 999–1007.

[12] Q. Wang, Q. Chen, G. Chen, and M. Zeng, "Numerical investigation on combined multiple shell-pass shell-and-tube heat exchanger with continuous helical baffles," *Int. J. Heat Mass Transf.*, Vol. 52, (2008), pp. 1214–1222.

[13] P. Stehlík and V. V. Wadekar, "Different Strategies to Improve Industrial Heat Exchange," *Heat Transf. Eng.*, Vol. 23, No. 6, (2002), pp. 36–48.